X-RAY APPARATUS

Discovered in 1896 by a German physicist Wilhelm Conrad Roentgen, X rays are an invisible and ionizing electromagnetic radiation. X rays consist of electromagnetic photons of energy $E = h\nu$, where ν is the photon's frequency and h the Planck constant. With much higher frequency than visible light, X-ray photons have much higher energy than visible-light photons. For example, in medical imaging, X-ray photon energies range from about 10 keV to 150 keV. Interacting with atomic electrons of body tissue, X-ray photons can be transmitted, scattered (deflected), or absorbed by atomic electrons of tissue. Absorption is also called photoelectric absorption, in which a photon is absorbed, a bound electron is released, and the atom ionized. Due to the scattering and absorption the incident X-ray intensity I_0 is attenuated, and the transmitted intensity I is given by

$$I = I_0 \exp[(-\mu/\rho)\rho t] \tag{1}$$

where μ/ρ and ρ are the mass attenuation coefficient and mass density of the tissue, respectively, and t is the thickness of the body part. Apparently, the transmission I decreases with increasing μ/ρ, ρ, and t. The mass attenuation coefficient μ/ρ and density ρ depend on the tissue composition. Bone has larger μ/ρ and ρ than soft tissue and thus attenuates more X rays than soft tissue does for comparable thickness. The mass attenuation coefficient μ/ρ of a given tissue depends also on photon energy. In general, the higher the photon energy, the smaller the μ/ρ. However, when photon energy reaches the binding energy of the atomic electrons of tissue, the photon absorption rate jumps up due to increasing atom ionization as does the mass attenuation μ/ρ. The photon energies at which μ/ρ jumps up are called the absorption edges. The existence of absorption edges is of great significance for designing X-ray imaging detectors and spectrum-shaping filters (discussed later).

Since X rays are an ionizing radiation, the quantity of radiation from X-ray exposure is better specified by the amount of ionization, more exactly, by the electric charge generated per unit mass of air. Therefore, the unit of X-ray exposure is defined as the roentgen (R), 1 R = 2.58×10^{-4} C/kg. In addition, an X-ray beam is also specified by "hardness," that is, by its penetrating ability. The beam-penetrating quality is specified by the half-value layer (HVL). The HVL of an X-ray beam is defined as the thickness of a metal attenuator that cuts the transmission exposure by half. From Eq. (1), for a beam of energy E

$$\mathrm{HVL} = \ln 2/\mu \tag{2}$$

where $\mu = (\mu/\rho)\rho$ at photon energy E and is called the linear attenuation coefficient of the attenuator. The higher the HVL, the more penetrating the beam. For medical imaging, the HVL of a beam is specified by the thickness of an aluminum attenuator. An X-ray-generating apparatus in medical imaging should generate an X-ray beam with a sufficiently high intensity (exposure rate) and a suitable HVL for imaging.

BREMSSTRAHLUNG AND CHARACTERISTIC RADIATION

X rays can be generated by the interaction of electromagnetic fields and charged particles such as electrons. Charged particles undergoing certain kinds of motion are able to generate electromagnetic radiation. A charged particle with a uniform motion of any velocity cannot radiate any energy in the form of an electromagnetic wave even though an electromagnetic field surrounds it. This is similar to a dc current in a broadcasting antenna that cannot radiate electromagnetic waves. Only a current of sufficiently high frequency in the antenna can radiate an electromagnetic wave. Similarly, only a charged particle undergoing sufficiently high acceleration or deceleration can emit X-ray radiation. That is why in current technology X rays are generated more often than not by energetic electrons bombarding a metal target.

When impinging on a metal target, the incident energetic electrons collide with atomic electrons and nuclei of the metal atoms. The incident electrons slow down and are continuously deflected in the metal target. The swift deflections are mostly caused by the electrostatic attraction between nuclei of the metal atoms and the incident electrons. These swift deflections subject incident electrons to huge momentum change, thus huge accelerations. Undergoing the acceleration, the incident electrons emit X rays, or electromagnetic radiation. Through repeated collisions with the metal atoms, the incident electrons eventually slow down and come to rest in the metal and loose their ability to cause the emission of X rays. The X-ray radiation generated in this way, by collision and slowing down of energetic electrons in metal, is called *bremsstrahlung* (literally, braking radiation in German).

Bremsstrahlung usually consists of X-ray photons of different wavelengths. In other words, bremsstrahlung is polyenergetic or polychromatic. The bremsstrahlung intensity I_n at a photon energy E, according to Kramers law, is

$$I_n = \begin{cases} \text{const} \times Z I_{\text{tube}}(E_0 - E) & \text{for } E < E_0 \\ 0 & \text{for } E \geq E_0 \end{cases} \tag{3}$$

where Z is the atomic number of the metal target, I_{tube} is the current of incident electrons, and E_0 is the highest photon energy in the bremsstrahlung. The highest photon energy E_0 is equal to the kinetic energy of incident electrons. In most X-ray generating equipment, the incident electrons are accelerated by an electrostatic potential before impinging on a metal target. Therefore, if the applied acceleration voltage for the incident electrons is 100 kV, then their kinetic energy is 100 keV, and the highest photon energy generated in the bremsstrahlung will be 100 keV. Put another way, for a bremsstrahlung, $E_0 = eV_0$, where V_0 is the applied acceleration voltage and, e is the electron charge. Thus Kramers law shows that below E_0 the spectral intensity increases with decreasing E (Fig. 1). However, taking into account the

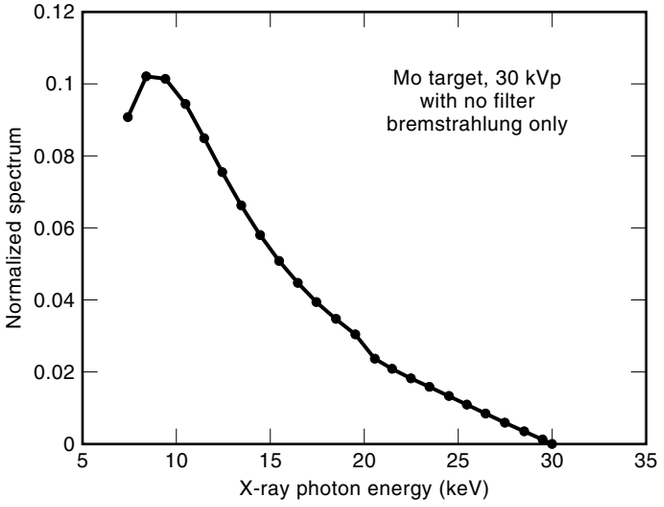

Figure 1. X-ray bremsstrahlung spectrum for a Mo-target at 30 kVp.

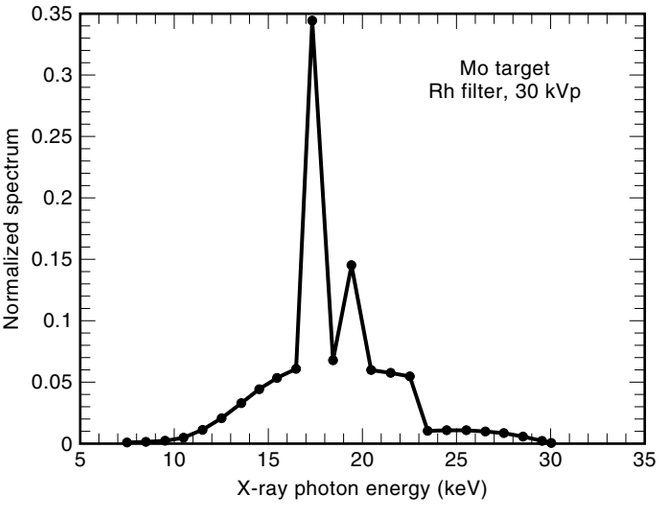

Figure 2. X-ray spectrum for a Mo-target and Rh-filter at 30 kVp.

attenuation of the X rays by the metal target itself, one finds the output bremsstrahlung peaks somewhere around $E_0/2$, depending on the target material and filtration (discussed later). The total bremsstrahlung intensity I of all photons is approximately given by

$$I = \text{const} \times ZI_{\text{tube}}E_0^2 = \text{const} \times ZI_{\text{tube}}V_0^2 = \text{const} \times ZPV_0 \quad (4)$$

where P is the power loading of tube. Equation (4) shows that the total bremsstrahlung intensity is approximately proportional to the square of the applied acceleration voltage and proportional to the electron current and the atomic number of the metal target material. Therefore, in order to increase X-ray bremsstrahlung output, one must apply a high acceleration voltage, increase the current, and use a high-Z target material. These three factors in fact are among the most important considerations in the design of X-ray-generating apparatus.

Bremsstrahlung is not the only method for X-ray generation. There is another important mechanism of X-ray generation with electrons bombarding the metal target. In fact, while colliding with atomic electrons of the target, the incident electrons can knock out atomic electrons from their atomic shell and cause inner-shell ionization of the metal atoms. With the return of the ionized atoms to their ground states, X-ray photons can be emitted. This kind of X-ray radiation is called characteristic radiation, because the energies of the emitted X-ray photons are discrete and equal to differences of the binding energy of the different atomic shells of the target material. Characteristic radiation is named after the relevant inner atomic shells such as K shell, L shell, and so on. For example, K characteristic radiation is generated when an electron is kicked out from the K shell and then the K shell is refilled. The characteristic radiation can only be generated when the energy of the incident electrons is larger than the binding energy of the corresponding atomic shell. In other words, characteristic radiation can only be generated when the applied voltage is above a certain value V_b (V_b is the binding energy of the atomic shell divided by the electron charge). The larger $V - V_b$ is, the greater the characteristic radiation. Therefore, the total X-ray output consists of bremsstrahlung and characteristic radiation, and the summed spectrum is shown in Fig. 2. The spikelike peaks in Fig. 2 are the superposition of these two kinds of X-ray radiation. For high-Z target material [such as tungsten (W)] bremsstrahlung dominates. But for lower-Z targets [molybdenum (Mo) or rhodium (Rh)], which are of significance for mammography, characteristic radiation plays an important role, as discussed later.

X-RAY TUBES

The implementation of the principle of x-ray generation as explained previously is relatively straightforward: an X-ray tube is a device with an electron emitter and a metal target; an X-ray generator supplies sufficient tube potential (acceleration voltage) and electron current. A modern X-ray tube consists of a cathode as the electron emitter, a rotating anode disk as the metal target, and a glass or metal envelope as a structural support (Fig. 3). The glass or metal envelope sus-

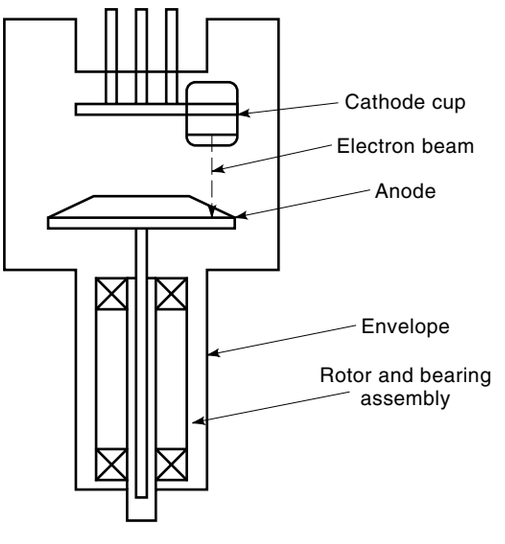

Figure 3. X-ray tube with a rotating anode.

tains a vacuum of about 5×10^{-7} Torr. For metal envelopes ceramic insulators are used as insulation between the envelope and the anode and cathode. The cathode is composed of a filament (a helically wound tungsten wire helix of 0.2 mm to 0.3 mm diameter) and a focusing cup. When heated to around 2400°C by the filament current, the hot filament emits electrons. Except for low tube potentials, the tube current I_A is almost independent of the tube potential and is a function of the filament temperature: $I_A = CT^2 \exp(-W/kT)A_f$. Here T is the temperature in K, W the filament's work function (for tungsten $W = 4.5$ eV), A_f the area of the filament, k the Boltzmann constant, and C a material-dependent constant. The higher the temperature, the larger the I_A. Usually the filament current is around 5 A for radiography and less than 4 A for fluoroscopy. However, for low tube potentials (<50 kV), not all the electrons emitted by the filament are drawn to the anode, and the tube current I_A is less than that predicted by this formula and becomes dependent on the tube potential. This behavior of I_A is called the *space-charge effect*. In fact, the low I_A limited by the space-charge effect (especially with small focal spots) imposes a technical challenge for mammography applications. Once emitted by the filament, electrons are accelerated by the high voltage across the tube to bombard the anode. The focusing cup focuses the electron beam so that the focal spot on the anode surface is kept small. A small focal spot ensures that the output X-ray seems to be emerging from a pinhole-like source, which is necessary for achieving good spatial resolution for X-ray imaging. In general a tube is equipped with at least two focal spot sizes. For tubes used in general radiography, typical focal spot sizes are 1 mm to 1.2 mm for large sizes, and 0.5 mm to 0.6 mm for small sizes. For tubes used in mammography, typical focal spot sizes are 0.3 mm for large sizes, and 0.1 mm for the small size. The anode is a rotating metal alloy disk. The target layer is tungsten (W) alloyed with 5% to 10% of rhenium (Re), and the remainder is graphite or molybdenum (Mo). The target material for mammography application is an exception and is either Mo or Rh. Note that the atomic numbers for W, Mo, and Rh are 74, 42, and 45, respectively. Equation (4) tells us that a W target would generate much more bremsstrahlung than a Mo or Rh target would do. The reason to use a Mo or Rh target in mammography is that the K characteristic radiation photons generated from these targets are in the range of 17 keV to 23 keV, which is optimal for breast imaging. The tube is encased in a lead-lined metal housing. In addition to the insert tube, the tube housing contains also a stator for driving the tube anode rotation (discussed later), high-voltage cable receptacles, and insulation oil. Therefore, the tube housing provides protection of the tube and high-tension electric insulation and prevents stray radiation leakage. In fact, the maximum allowed stray radiation leakage from the tube housing is federally regulated in the United States. The insert tube and tube housing together are called the X-ray tube assembly. Recently, single-tank tube assemblies were also developed for portable or low-power radiography units in which the tube is integrated with a high-frequency X-ray generator (discussed later).

The anode disk materials should also have a high melting point and good thermal conductivity. About 99% of the input energy is transformed into heat in the anode, due to the collisions between incident electrons and target atoms, as discussed previously. The temperature is not uniform in the anode during exposure, with the focal spot hotter than the focal track, which is hotter than anode body. This is so because the anode is rotating during exposure. The anode as a rotor is driven by the stator through magnetic induction, running as an asynchronous motor. The stator itself is fed by a driving current from the high speed starter of the generator. The anode rotation speed ranges from 1,200 revolutions/min to 3,600 revolutions/min for normal speed modes and can go as high as 10,800 revolutions/min for the high-speed mode. Operating "dry" in a vacuum at such a high temperature, the ball bearing must satisfy some exceptional specifications. To extend its life, the anode rotates only before each exposure, and thereafter it is brought to rest by a braking circuit of the generator. The electron-impact time decreases with ωr, where ω is the anode angular velocity and r the anode radius. Therefore, the focus-spot temperature increases with the input power and X-ray exposure time, and decreases with increasing focal-spot size, rotation speed, and anode diameter. The practical limit of the focal-spot temperature is 2500°C (although tungsten's melting point is 3370°C, the highest of all metals), thus each X-ray tube has its own maximum allowed power loading, which is called the tube power rating. In general, the average power loading (in watts) for an X-ray tube during an exposure is determined by

$$\text{Power loading} = w \times (\text{tube potential}) \times (\text{tube current}) \quad (5)$$

where the tube potential is in kV and the tube current in mA, w is the tube potential wave-shape factor, $w = 0.99$ for three-phase 12-pulse, or high-frequency generators, $w = 0.95$ for three-phase, six-pulse generators, $w = 0.74$ for single-phase generators, because the tube potential is defined as the peak voltage across the tube and the current as average current (discussed later), and the tube current is measured in milliamps. The tube power rating increases with increasing focal-spot size, rotation speed, and anode diameter. For example, since high tube power loading is required for digital subtraction angiography (DSA) applications as explained before, a tube with large diameter (5 in. to 9 in.) anode disk is desired. Note that for a given tube with a given rotation speed and focal-spot size, the tube power rating decreases with increasing exposure time. One can find power ratings for different exposure times from the manufacturer-supplied tube rating chart or the so-called single-exposure rating chart. For radiography and fluoroscopy applications, the tube power rating is usually 100 kW and 30 kW for a 0.1 s exposure with an anode rotation of 10,800 revolutions/min, and a focal spot of 1.2 mm and 0.6 mm, respectively. In addition to the power rating, X-ray tubes are also specified by the anode heat capacity, the maximum anode heat load allowed. A large anode mass increases anode heat capacity. The heat load generated during an exposure, expressed in heat units (HU, 1 J = 1.35 HU), is equal to $1.35 \times$ (power loading) $\times$ (exposure time, in seconds). For radiography and fluoroscopy applications, tube anode heat capacity usually is not less than 400 kHU. For X-ray tubes in computed tomography (CT) applications, while the power loading is not high, the heat loading is high. The anode heat capacity for CT typically ranges from 2 MHU to 4 MHU. For newly developed CT fluoroscopy, the anode heat capacity can be as high as 6.5 MHU or more. In fact, the tube anode heat capacity become a bottleneck for spiral CT scans. Tube heating during multiple exposures depends also on heat dissipation.

In fact, the anode cools by radiating heat. A large anode surface and emissive coating increase heat dissipation. In addition, the tube housing also has its own maximum allowed heat load. Exceeding the housing maximum heat load can cause failure of the housing or the tube due to thermal expansion of the insulating oil surrounding the tube. For some DSA applications, a tube assembly may be equipped with external oil to air or oil to water heat exchangers for fast cooling.

For X-ray imaging another device associated with an X-ray tube assembly is the filter. A filter is a metal sheet used to shape the output X-ray spectrum. During an exposure, there are low-energy photons in the bremsstrahlung as shown in Fig. 1. These low-energy photons will be absorbed by patient's body before reaching the imaging detector and hence do not contribute to the imaging. As explained before, the penetrating ability of a beam is specified by the HVL. The higher the HVL, the more penetrating the beam. In order to reduce the radiation dose to the patient during imaging, the beam minimum HVL allowed at a given tube potential in kilovolts (kVp) is regulated in United States. An aluminum filter can reduce the number of low-energy photons and thus raise the output beam's HVL. Usually an aluminum filter of 1 mm or more in thickness is used for this purpose. Sometimes, especially for the angiography of heart or body, a copper filter of 0.1 mm or more in thickness is used. For mammography, absorption-edge filters are used to shape the beam spectrum. As explained before, at the absorption edge the mass attenuation μ/ρ jumps up. Using an absorption-edge filter, one can selectively attenuate photons with energy higher than the absorption edge, hence shape the output X-ray spectrum. For example, Mo has an absorption edge at 19.97 keV and Rh at 23.19 keV. Using a Mo filter or a Rh filter with an X-ray tube of a Mo-target, one can make more output photons with the optimal energy range for breast imaging.

X-RAY GENERATORS

The main function of an X-ray generator, as mentioned before, is to provide controllable high tube potentials and high tube currents for tube operation. A generator is specified by the kVp rating (the maximal kVp allowed), the tube potential ripple (kV ripple) and the power rating (the maximal power loading allowed for a 0.1 s exposure.) Here the kVp means the peak tube potential in kilovolts. During an X-ray exposure, the tube potential is not a strict constant but fluctuates around a certain value. The amount of the kV ripple is usually specified as the percentage of the kVp during exposure. As discussed earlier, the kVp value determines the highest photon energy available in the output X-ray beam. Note that the scattering and absorption of X-ray photons by a patient are dependent on photon energy. Therefore, knowing kVp and the amount of ripple during an exposure is necessary for an estimate of the beam spectrum and important for optimizing the imaging technique and calculating the radiation dose of the patient. Apparently, a generator with less kV ripple is better, since the tube potential is better controlled, more consistent, and repeatable. This is important for consistency of the X-ray image quality. In general, the higher the kVp, the more penetrating the X-ray beam, but the lower the image contrast. The kVp value used for medical imaging thus varies according to the application. Typical tube potentials are, for example, 125 kVp to 150 kVp for chest X-rays, 110 kVp to 130 kVp for computed tomography, 75 kVp to 85 kVp for abdomen exams, 65 kVp to 75 kVp for skull exams, and 25 kVp to 35 kVp for mammography. Therefore, typical kVp ratings are $\leq$150 kVp for radiography and fluoroscopy (RF) generators and $\leq$45 kVp for mammography generators. The typical power ratings are 60 kW to 100 kW for DSA generators, 50 kW to 60 kW for the RF generators, and about 5 kW for mammography generators. Note that the DSA needs a relatively low kVp (for good image contrast) but high beam intensity (for less quantum noise, discussed later). Equation (5) thus suggests a high power rating needed for the DSA generators.

As discussed earlier, the heart of an X-ray generator should be a high-power and high-voltage circuit. A basic single-phase generator is shown in Fig. 4. The auto-transformer TF1, which is fed by the line ac power, functions as the output kVp selection. The high-voltage transformer HTF transforms the low ac voltage to high voltage ac. The diode bridge rectifies (full-wave) the high-voltage ac. The step-down transformer TF2 provides filament current selection for the filament. Note that the filament current can be more than 5 A. From the rectified sine-wave form it is clear that the kV ripple can go as high as 100% with a single-phase generator. As discussed above, such a large kV ripple will generate many low-energy photons, which contribute nothing to imaging but radiation dose to the patient. An improvement can be achieved if the line supply is replaced by a three-phase line supply. In this case, the rectified sine waves from different phases can be interleaved, and kV ripple can thus be reduced to 13% to 25% (for six-pulse interleaving) and 5% to 10% (for 12-pulse interleaving.) A disadvantage of single- or three-phase generators is that the generated kVp also depends on line regulation, and the kVp reproducibility is easily compromised by unstable line-supply conditions. In addition, single- or three-phase generators have a slow time response.

Single- and three-phase generators, especially the high-voltage transformer, are bulky both in size and weight. Since the induced voltage in a transformer is proportional to the product of core cross section A, the number of turns n, and operating frequency f, a generator operating at high frequency allows reduction in A and n. Therefore, a generator operating at a high frequency can be much smaller and lighter. This is why high-frequency generators, operating at a frequency of a few to tens (even about one hun-

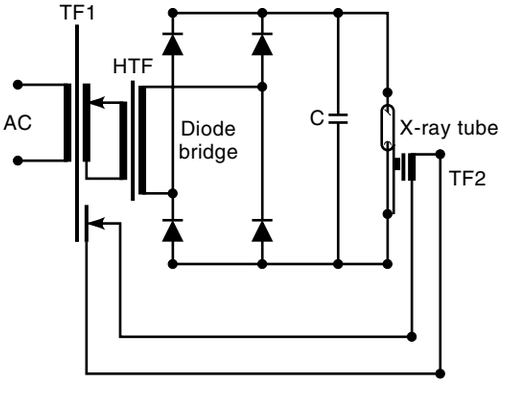

Figure 4. Basic circuit diagram of a single-phase X-ray generator circuit.

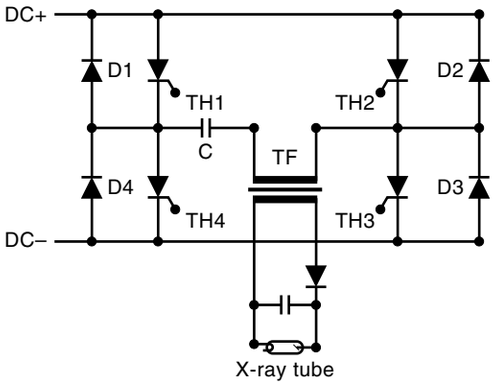

Figure 5. Basic circuit diagram of a high-frequency inverter circuit.

dred) kilohertz have become popular in recent years. Compared with single- and three-phase generators, high-frequency generators are smaller in size and weight by 50% to 80% and reduce manufacturing costs a lot. More important, high-frequency generators provide fast response and much smaller kV ripples. High-frequency generators are based on converter technology, by which the incoming 60 Hz few hundred volt ac power is rectified and filtered to a dc power, and the dc power is then inverted to high frequency (HF) pulses. A basic dc to HF inverter is shown in Fig. 5. Four thyristors TH1 to TH4 work as controlled switches. In a sense, a thyristor is a diode with a control gate. The trigger pulses applied to the gate of a thyristor control the on and off switching of the current flowing through the thyristor. The high-voltage transformer TF, which steps up voltage, couples the X-ray tube as a load to the inverter and provides the needed high voltage to the tube. The coupling capacitor C, the inductance L of transformer TF, and the load from the tube consists of a series *RLC* resonant circuits controlled by "switches" TH1 to TH4. When, for example, thyristors TH1 and TH3 are gated on, just like the two switches are closed, the dc voltage is applied to the *RLC* circuit. The capacitor C initially opposes the change in voltage and the inductor L resists the current change, because capacitor C stores electric energy and inductor L stores magnetic energy. The interchange of electric and magnetic energy and energy dissipation on the load R result in a dampened sinusoidal current in the thyristors and *RLC* circuit. This is similar to an interchange of kinetic energy and potential energy, which causes a swinging movement. The frequency of the sinusoidal current in the *RLC* circuit is called the resonant frequency and is equal to

$$f_{\text{res}} = 1/[2\pi(\text{LC})^{1/2}] \tag{6}$$

During the negative half of the sinusoidal cycle, the *RLC* circuit current flows through the antiparallel diodes D1 and D3 instead of thyristors TH1 and TH3, since thyristors do not allow a reverse current. Note that the dampening of the load makes the second peak smaller than the first in the cycle. When the full cycle is completed, the *RLC* circuit would try to start its second cycle; however, the thyristors TH1 and TH3 have already been switched off (self-communication) during the reversing half cycle. For each pair of trigger pulses to the gates of TH1 and TH3, only a single current pulse is generated (Fig. 6). For degaussing the transformer core, the next current pulse is generated by gating on thyristors TH2 and TH4. Since the polarity of the applied dc power is reversed this time, the *RLC* resonance process leads to a "reversed" current pulse. The time delay between the two pulses is controlled by how often the two trigger-pulse pairs are applied. The frequency with which the two trigger-pulse pairs are applied is called the driving frequency f_{d}. The higher the driving frequency, the denser the current pulse train. The secondary coil of the transformer TF couples a rectifying circuit with the *RLC* circuit. The rectifying circuit consists of a diode bridge and the load capacitor C_1 for filtering. The tube potential is equal to the voltage across C_1. The rectifying circuit transforms the high-frequency current pulses into charge packets stored in C_1. At the beginning of an exposure, f_{d} is very high such that C_1 is charged quickly and the desired tube potential is built up. The voltage of C_1 can be measured by a precision resistor voltage divider. Once the desired voltage is established, a feedback signal is sent to the voltage–frequency converter V/F, whose output controls the driving frequency f_{d} of the gate trigger pulse circuit. The f_{d} is lowered to deliver just enough charge packets to C_1 for compensating the discharge caused by the tube current. Therefore, while the resonant frequency is fixed by C and L through Eq. (6), the driving frequency varies during exposures. But the maximum driving frequency allowed is the resonance frequency f_{res}. Due to the closed-loop servo control described previously, the tube potential control is very fast and accurate, and the kV ripple can go as low as 2%. Note that the kV ripple also depends on power, ranging from 2% to 15%. For a given resonant frequency f_{res}, the ripple decreases with increasing power. In order to keep kV ripple uniform, an X-ray generator may have to use different coupling capacitors when power levels change (say, from large-focal-spot mode to small-focal-spot mode). In addition, since the inverter circuit is powered by a dc power supply, high-frequency generators can use either a single- or three-phase line supply.

The inverter circuit just described can also be used for filament power supply. A filament inverter functions like the inverter for generating high voltage. The major differences are as follows. The filament transformer steps down the voltage (steps up the current), and the secondary coil of the transformer is coupled directly to the tube filament without rectifying circuitry. The real tube current generated is sensed by a precision resistor in series with the tube, and this signal is used as the feedback signal for the driving-frequency control.

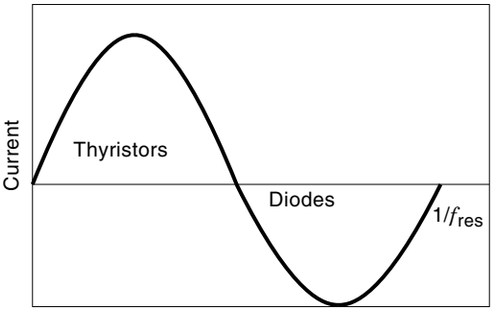

Figure 6. Current pulse waveform in a high-frequency inverter.

This method of tube current control is faster and more accurate than that in single or three-phase generators.

In addition to the high-voltage power circuitry as described earlier, an X-ray generator includes circuitry to control the amount of radiation delivered. It is clear from Eq. (4) that the radiation exposure rate is proportional to tube current I_{tube} for a selected kVp value. Hence the amount of radiation exposure is proportional to the integral of I_{tube} over the exposure time, which is called the total mAs value (milliamps times seconds) of the exposure. All X-ray generators include an mAs switch to control the total mAs delivered during an exposure. A variety of mAs switch circuitry is available, ranging from a simple electronic timer (for a constant current during exposure), to a current integrator (for a falling I_{tube} during exposure), to an automatic exposure control (AEC) circuitry, in which exposures are turned off when a preset amount of radiation incident on the image receptor is reached. The AEC circuitry finds wide applications in medical imaging, since it ensures that the imaging detector always receives almost the same amount of radiation exposure in spite of the difference in X-ray attenuation with different patients. A typical AEC circuit consists of a radiation sensor that generates a current proportional to the exposure rate incident on the image receptor, a current integrator that measures the exposure to the image receptor, and a comparator that sends out the exposure termination signal when the output of the current integrator reaches the preset value. The radiation sensor is usually an ionization chamber that transforms the X ray to an electric current, or a fluorescent screen coupled with a phototube or photodiode, in which the screen transforms the X ray to light (discussed later) and the phototube or photodiode works as a light sensor. This is why AEC circuitry is also called a phototimer.

APPARATUS FOR PROJECTION RADIOGRAPHY

Projection radiography is the most conventional technique used in radiological imaging. It uses an X-ray beam to generate a two-dimensional transmission image of the patient anatomy. Since Roentgen produced the first projection radiograph more than 100 years ago, the technique has been widely used for a large variety of examinations, such as bone, chest, and breast. In the past few decades, many technically advanced imaging modalities, such as CT and MRI, were introduced into clinical practice. The conventional projection radiography methods remain, up to now, the most popularly used tools in diagnostic imaging.

Projection radiograph is a transmission-imaging technique. As shown in Fig. 7, during X-ray exposure, the X-ray beam passes through the body of the patient and is recorded by a two-dimensional detector. In passage, the X-ray radiation is attenuated by absorptions and scattering within the body. Different anatomical structures, as well as different body thicknesses, attenuate the X-ray beam differently. The projection radiograph is therefore a spatially modulated attenuation pattern of the anatomical structure. In other words, a projection radiograph is a two-dimensional "X-ray shadow image" of the three-dimensional anatomy of the patient.

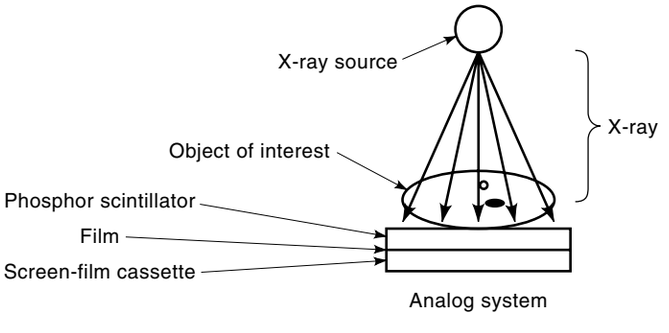

Figure 7. Schematic of projection radiograph.

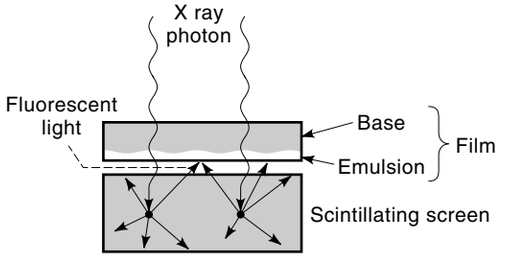

Figure 8. Screen–film combination as an analog detector in radiography.

Film was the first radiographic detector used in medicine and up to now it is still widely used in medical imaging. In fact, the function of a radiographic film is not only as a detector, it simultaneously plays the role of a display device and an archiving medium.

The unexposed film is a thin sheet of inert plastic coated with emulsion on one or both sides. The film is insensitive to X-ray energies used in medical practice. Therefore, the X-ray images are, in most cases, detected in a two-step process with a screen–film combination. Here the term *screen,* also called intensifying screen, refers to a scintillating screen that contains densely packed fluorescent material of high atomic number.

Figure 8 shows a screen–film device for projection radiography. A piece of film is placed in direct contact with a piece of intensifying screen in a cassette. During X-ray exposure, the X-ray photons emitted from the patient first interact with the intensifying screen. The X-ray photons undergo a photoelectric or Compton collision and generate a large number of visible-light photons. These light photons then strike the film. With a subsequent chemical development process, the original radiographic image of the patient is captured permanently on the film.

As we discussed in the preceding section, analog projection radiography uses a scintillator and film to record images. In contrast, digital radiography generally uses electronic detectors to record images. Various electronic and/or optoelectronic detectors were developed and have been successfully applied in clinical practice. In the following, we take an optically coupled charge-coupled device (CCD) system as an example to describe the operation of digital radiography.

Figure 9 is a schematic of an optically coupled CCD that was designed for spot compression mammography (small-field breast image for breast-cancer detection and diagnosis) (1–4).

An optically coupled CCD X-ray imaging system primarily consists of a two-dimensional CCD imager, an optical coupler (such as a large-aperture photographic lens or a spatially coherent optical fiber taper), and a scintillating screen. During X-ray exposure, the X-ray beam passes through the patient,

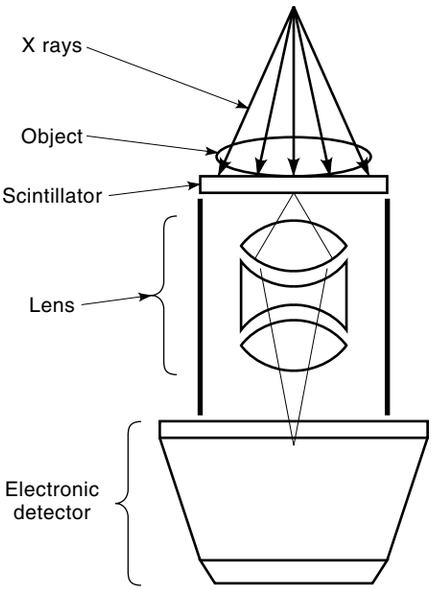

Figure 9. Schematic of a lens-coupled CCD X-ray imaging system.

is attenuated, and interacts with the scintillating screen. Here the X-ray photons are converted into a large number of light photons and the resultant light photons form an optical image. The optical image is demagnified by the lens or optical-fiber taper and projected onto the photosensitive surface of the CCD. The CCD pixel array samples the optical input, creating an electronic image. The CCD output is digitized by an analog-to-digital convertor. The digital image is then sent to a computer or a digital image processor for analysis, manipulation, and transmission. The digital image can be stored in magnetic or optical media. The digital image can be transferred back into analog signal form for video display. The digital data can also be printed on film using a high-resolution laser imager.

SIGNAL-TO-NOISE RATIO ANALYSIS OF RADIOLOGICAL IMAGING

In radiological imaging, X-ray quantum efficiency and corresponding imaging characteristics such as the signal-to-noise ratio (SNR), noise power spectrum (NPS), and detective quantum efficiency (DQE) are crucial to design considerations and performance evaluations such as lesion detectability and patient radiation dose. The following modeling of SNR, NPS, and DQE will provide a comprehensive summary of both theoretical and practical aspects of the radiological imaging apparatus. Here we use the optically coupled CCD system described in the previous section as an example for analysis. The concept can be applied to many other radiological imaging systems. In an optically coupled CCD X-ray imaging system (no image intensifier in the imaging chain), the transfer of light from an X-ray intensifying screen to a CCD imager can be accomplished by directed contact of these components. However, currently available CCDs require a demagnifying optical coupler (either a lens or fiber taper) between the intensifying screen and the detector to image an area larger than the size of the detector.

In the quantum transfer of image data between an intensifying screen and imager, the optical coupling component represents a weak link in the cascaded imaging chain. Thus, in the 1960s and 1970s, image intensifiers were considered integral components for achieving quantum noise limitation in electronic imaging systems (5,6,7). To determine whether this assumption holds for newer electronic detectors, we derived an equation for analyzing the signal-to-noise ratio for these systems.

The noise in an optically coupled CCD system is composed of quantum noise (X-ray quantum noise and secondary quantum noise generated through the cascaded process) and additive noise (noise related to the detector or to the detector electronics). Although each noise component can be analyzed separately using existing mathematical methods (8), we have derived a SNR equation encompassing the combined effects of both quantum and additive noise (9). The equation was derived based on the principle of cascaded imaging analysis and other SNR models (8,10). Although it can be applied to many imaging systems, this equation is particularly convenient for analyzing performance or optimizing design tradeoffs for optically coupled CCD X-ray imaging systems. The details and derivation of this equation can be found in Ref. 9.

$$\mathrm{SNR} = C(\eta N_\mathrm{i})^{1/2}[1 + 1/g_1g_2 + 1/g_1g_2g_3 + N_\mathrm{a}^2/(g_1g_2g_3)^2\eta N_\mathrm{i}]^{-1/2} \tag{7}$$

where η is the quantum efficiency of the intensifying screen or other scintillator used in the imaging chain. It is assumed that all the statistical processes of absorption, photon transport within the screen, and photoemission can be described and characterized by one number, the quantum efficiency h (8).

Also N_i is the X-ray photon flux, which is the number of X-ray photons per pixel at the entrance of the intensifying screen; N_a is the total additive noise of the overall imaging chain; g_1 is the X-ray to light conversion ratio, or quantum gain of the intensifying screen; g_2 is the optical coupling efficiency of the lens, fiber taper, or other coupler; g_3 is the quantum efficiency of the CCD or other electronic detector; and C is the subject contrast.

The product of $g_1g_2g_3$ is the overall quantum efficiency or total quantum gain of the system; its unit is the number of electrons produced in the CCD per X-ray photon absorbed in the scintillator (electrons per X-ray photon).

The quantum efficiency of a standard mammographic screen has been estimated at $\eta = 0.65$ (11). Assuming a typical mammographic screen entrance exposure of 12 mR and an average X-ray photon energy of 20 keV, the number of X-ray photons per pixel at the entrance of the intensifying screen, for a detector having a 0.048 mm $\times$ 0.048 mm pixel size, is $N_\mathrm{i} = 1600$ X-ray photons/pixel. Therefore, the number of absorbed X-ray photons per pixel is $\eta N_\mathrm{i} = 1040$ X-ray photons/pixel. For this analysis, a contrast (C) of 1 was assumed. For a system using a cooled CCD, the total additive noise N_a is usually less than 15 electrons; for TV tubes, N_a is usually larger than 500 electrons. The data for the CCD are from the manufacturer's data sheet (Photometric, Inc., Tucson AZ); TV tube (Vidicon) data were compiled from several review papers (12–14). The X-ray to light conversion ratio (g_1) of a high-resolution mammography intensifying screen is reported at 400 to 600 in the forward direction (15). Conservative esti-

mates of g_3 are (1) 0.35 for a front-illuminated CCD, (2) 0.60 for a back-illuminated CCD such as the Tektronix (TK2048EB), and (3) 0.20 for a TV tube. From our previous work (16), we have estimated the optical coupling efficiency of a lens to be

$$g_2 = 0.75/[4F^2(1+M)^2+1] \tag{8}$$

where F is the F number (the ratio of the focal length to the effective diameter) of the lens and M is the demagnification ratio. For instance, for an $f/0.8$ (f = 0.8) lens working at a demagnification factor of 2, g_2 = 3.1%. Equation (7) can be used to illustrate the dominant noise component in a cascaded electronic imaging system. For instance, if the total quantum gain $g_1g_2g_3$ of the imaging chain is small or the additive noise N_a is large, the value of the denominator is larger than 1. Then the SNR of the system is dominated by one of the cascaded stages or by additive noise. While $g_1g_2g_3$ is small, the additive noise N_a will affect the performance of the system significantly. As $g_1g_2g_3$ becomes large, the value of the denominator approaches 1 and the equation reduces to SNR = C/hN_i, representing a perfect X-ray quantum-noise-limited, additive noise-free imaging system.

To illustrate an example application of Eq. (7), we use parameters typical for lens-coupled TV camera systems, which were extensively investigated in the 1960s and 1970s. Substituting $g_1g_2g_3$ = (500)(0.031)(0.2) = 3.1 and N_a = 500 into Eq. (7) we have

$$\text{SNR} = C(\eta N_i)^{1/2}/(1.32+25)^{1/2} = 0.2C(\eta N_i)^{1/2} \tag{9}$$

This example illustrates that the lens-coupled TV system is not X-ray quantum-noise limited and that it is the additive noise (N_a) not the total quantum gain ($g_1g_2g_3$) that dominates the SNR.

The introduction of the image intensifier (II) provided a solution to the additive-noise problem by boosting the image signal and increasing quantum gain. The value for $g_1g_2g_3$ may approach 400, and therefore the SNR of an II-TV system can be expressed as

$$\text{SNR} = C(\eta N_i)^{1/2}/(1+0.004)^{1/2} = 0.99C(\eta N_i)^{1/2} \tag{10}$$

The II-TV system is absolutely X-ray quantum-noise limited, and both analog and digital II-TV systems are used currently in many clinical procedures. However, electro-optical devices such as image intensifiers have limitations that reduce spatial resolution and contrast sensitivity. Mammography, which requires high spatial resolution and high contrast sensitivity, cannot be performed using a conventional II-TV system. Examining Eqs. (1) to (4) more closely, it is theoretically intuitive that X-ray quantum-noise limitation might be achieved *without* an image intensifier if the additive noise level were greatly reduced. Modern CCD receptors, having additive noise as low as 15 electrons, are suitable detector candidates. For current CCD devices, a typical total quantum gain can be expressed as $g_1g_2g_3$ = (500)(0.031)(0.6) = 9.3 electrons per X-ray photon.

Thus Eq. (1) becomes

$$\text{SNR} = C(\eta N_i)^{1/2}/(1.1+0.002)^{1/2} = 0.95C(\eta N_i)^{1/2} \tag{11}$$

Table 1. Total Quantum Gain, Additive Noise, and Their Impact on SNR

	Lens-TV	II-TV	Lens-CCD
Additive noise N_a (electrons)	500	500	15
Quantum gain $g_1g_2g_3$ (electrons per x-ray photon)	3.1	400	9.3
SNR	0.2 $(\eta N_i)^{1/2}$	0.99 $(\eta N_i)^{1/2}$	0.95 $(\eta N_i)^{1/2}$

For a cooled CCD system, the degradation in SNR caused by the cascaded stages and the additive noise are nearly negligible, illustrating that an optically coupled CCD imaging system can indeed be X-ray quantum-noise limited.

Assuming a contrast (C) of 1 and a constant phosphor noise level for all three systems, the preceding analysis can be summarized as shown in Table 1. Note that in this table, the value of $g_1g_2g_3$ for the lens-TV was calculated assuming the quantum efficiency of the TV tube is 0.2. The value of $g_1g_2g_3$ for the lens CCD was calculated assuming the quantum efficiency of a back-illuminated CCD to be 0.6.

Figure 10 plots the relationships of SNR to the total quantum gain (electrons per X-ray photon) and total additive noise (electrons) for three detector systems and illustrates that a total quantum gain of 10 electrons per absorbed X ray makes a CCD imaging system X-ray quantum-noise limited in the low-frequency range. According to our calculations and experiments, it is feasible to design a lens-coupled or a fiber-optically coupled CCD X-ray imaging system to meet these requirements under clinical conditions. In comparison, other electronic detectors have noise levels of a few hundreds or even a thousand electrons (13). To achieve X-ray quantum-noise limitation under these conditions, a total quantum gain of 100 to 200 electrons per absorbed X-ray photon is needed.

Noise power spectrum (NPS) analysis of image noise and noise transfer provides a complete description of noise. When characterizing the noise properties of real or proposed digital mammographic systems experimentally, we calculate the NPS directly from the noise fluctuations using the fast Fourier transform (FFT):

$$\text{NPS}(f_x, f_y) = \text{FFT}_{2D}[N(x,y)] \tag{12}$$

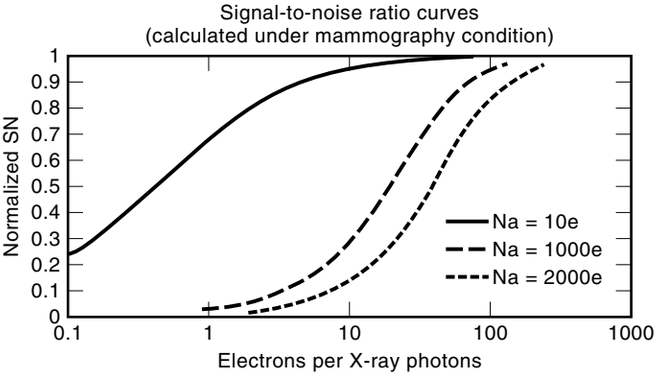

Figure 10. Normalized SNR curves plotted as functions of total quantum gain (electrons per X-ray photon) and additive noise (electrons).

where FFT_{2D} represents the fast Fourier transform in two dimensions (2D) and $N(x, y)$ is a two-dimensional data array of noise fluctuation or a so-called "noise-only" image. This image is acquired using the following procedure:

1. Acquire images $A(x, y)$ and $B_1(x, y)$, . . ., $B_{50}(x, y)$ under identical conditions simulating clinical mammography procedures. A Lucite slab of 4.5 cm thickness is used and the entire imaging field is uniformly irradiated.
2. Determine the "noiseless" image as an average of 50 images:

$$\langle B(x, y)\rangle = 1/50 \sum B_n(x, y) \tag{13}$$

3. Calculate $N(x, y) = A(x, y) - B(x, y)$ as the difference between the single image $A(x, y)$ and the noiseless image; $N(x, y)$ is the noise-only image we are seeking.
4. $NPS(f_x, f_y)$ is a two-dimensional data array in the frequency domain. We assume the proposed CCD imaging system to be symmetric in the x and y directions; therefore, as a slice of the data, $NPS(f_x)$ is taken to evaluate the noise properties of the whole image.

Repeating this procedure 20 times ($n = 20$), 20 $NPS(f_x)$ curves are generated. Furthermore, the $NPS(f_x)$ is normalized with respect to its value at zero frequency, making the value at zero frequency equal to 1, the normalized noise power spectrum NPS′ is given by

$$NPS'(f_x) = 1/20 \sum NPS(f_x)/NPS(0) \tag{14}$$

The averaging process in Eq. (8) is usually necessary to avoid statistical uncertainty. The preceding discussion on the noise power spectrum provides a foundation for understanding the concept of noise propagation in a cascaded imaging chain and its relation to the signal-to-noise ratio and detective quantum efficiency. The measured NPS curves of various optically coupled CCD X-ray imaging systems can be found in the literature (17,18).

The detective quantum efficiency (DQE) expresses the SNR transfer characteristics of an imaging system as a function of the spatial frequency (17,19,20):

$$DQE(f) = SNR^2_{out}(f)/SNR^2_{in}(f) \tag{15}$$

where $SNR_{out}(f)$ is the output signal-to-noise ratio and $SNR_{in}(f)$ is the input signal-to-noise ratio. The $DQE(f)$ provides a measure of how efficiently the imaging system transfers information in terms of spatial frequency. In order to determine $DQE(f)$, we conducted the following derivation:

$$\begin{aligned} SNR^2_{out}(f) &= S^2_{out}(f)/NPS(f) \\ &= S^2_{out}(0)MTF^2(f)/NPS(0)NPS'(f) \\ &= SNR^2_{out}(0)MTF^2(f)/NPS'(f) \end{aligned} \tag{16}$$

where $S_{out}(f)$ is the output signal, which can be expressed as the product of its zero-frequency value, $S_{out}(0)$, and $MTF(f)$, the norm of the system transfer function (21). Similarly, the $NPS(f)$ can be expressed by its normalized form, $NPS'(f)$, and the normalization factor NPS(0).

Assuming the input X-ray quanta obey Poisson statistics and have a flat noise spectrum within the range of the spatial frequency of practical interest, then

$$SNR^2_{in}(f) = SNR_{in}(f) = CN_i \tag{17}$$

where N_i is the incident X-ray photon flux (number of X-ray photons per pixel at the entrance of the intensifying screen). Thus

$$DQE(f) = DQE(0)\,MTF^2(f)/NPS'(f) \tag{18}$$

where the ratio $MTF^2(f)/NPS'(f)$ provides a spatial frequency modulation term for DQE.

DQE(0) can be determined using the following method. We have shown that, at zero frequency, repeating Eq. (7),

$$\begin{aligned} SNR_{out}(0) &= C(\eta N_i)^{1/2}/[1 + 1/g_1g_2 + 1/g_1g_2g_3 \\ &\quad + N_a^2/(g_1g_2g_3)^2\eta N_i]^{1/2} \\ SNR_{in}(f) &= CN_i^{1/2} \end{aligned} \tag{19}$$

Therefore

$$\begin{aligned} DQE(0) &= SNR^2_{out}(0)/SNR^2_{in}(0) \\ &= \eta/[1 + 1/g_1g_2 + 1/g_1g_2g_3 + N_a^2/(g_1g_2g_3)^2\eta N_i] \end{aligned} \tag{20}$$

Analyses of DQE(0) and of SNR at low frequency provide a useful tool for evaluating design tradeoffs for electronic X-ray imaging systems, such as the choice of scintillator, optical coupling techniques, and electronic imagers.

Using Eq. (20), the DQE(0) values for several electronic X-ray imaging systems were plotted as a function of total quantum gain ($g_1g_2g_3$) and the additive noise (N_a) in Fig. 11. For a low-additive-noise system, such as the optically coupled CCD, a total quantum gain of 10 electrons per X-ray photon brings the DQE close to its maximum value. Further increasing the total gain will not improve the DQE significantly. This analysis applies to the low-frequency range. To preserve high-frequency DQE and to ensure that the system is X-ray quantum-noise limited at high frequencies, a total quantum gain of 10

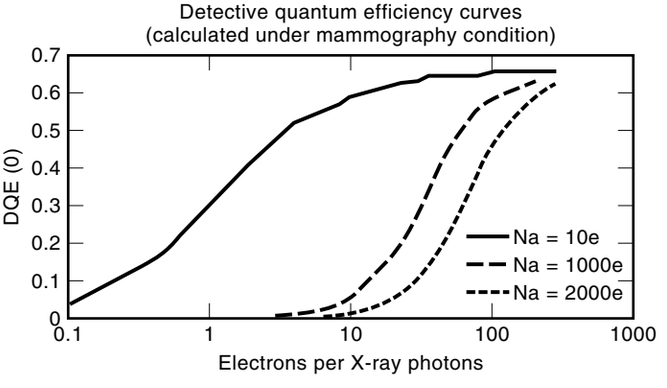

Figure 11. Detective quantum efficiency curves plotted as functions of total quantum gain (electrons per X-ray photon) and additive noise (electrons). The quantum efficiency of the scintillating screen was assumed to be $h = 0.65$. Note that the DQE values presented in this figure are the maximum achievable values.

electrons per X-ray photon is again required (17). These guidelines have been used in developing both lens and fiber-optically coupled CCD systems. For a lens-coupled prototype, a large aperture lens was custom designed and a back-illuminated CCD used. The back-illuminated CCD has a quantum efficiency nearly 2 times greater than a front-illuminated CCD and meets the required 10 electrons per X-ray photon. A fiber-optically coupled CCD could be designed with a total quantum gain that is much higher than 10 electrons per X-ray photon due to the high efficiency of the optical fiber (4). In a practical design tradeoff, however, we selected an optical-fiber component with heavy extramural absorption material, having only moderate efficiency in return for improved contrast and lower cost (22). The curves presented in Fig. 11 also shows that 100 to 200 electrons per X-ray photon are needed to maximize the DQE for other electronic imaging systems with higher detector noise. The flat panel imagers capable of converting X-ray photons directly to electrons could potentially provide a high total quantum gain and are under development currently (23).

The quantum efficiency (η) of the scintillating screen plays an important role in the DQE and radiation efficiency. According to Eq. (20), the maximum achievable DQE of an X-ray quantum-noise-limited system is limited primarily by h. In practice, a variety of scintillating screens are used in radiological imaging. In a couple of our early optically coupled CCD spot mammography systems (2,5), Min-R screens with a quantum efficiency of 55% to 65% (η = 0.55 to 0.65) were used. Recently developed cesium iodide crystals offer a higher efficiency (η = 0.90 or higher), leading to a higher system DQE (24). In Fig. 12, the DQE(0) curves of two optically coupled CCD mammographic systems are plotted as a function of total quantum gain and the quantum efficiency of the scintillating screen. (Note that the DQE values presented in this figure are the maximum achievable values). This figure demonstrates that the scintillating screen used will affect the DQE of the overall system significantly.

We wish to emphasize that the SNR analyses discussed in this article are based on single pixel values (X-ray photons per pixel, electrons per pixel). Single-pixel analysis is useful and convenient for determining if an imaging system is X-ray quantum-noise limited, but is not valid for lesion-detectability evaluations. The Rose model (25,26) or quasi-ideal signal-to-noise ratio (27,28) are more appropriate for these types of analyses. The methods presented here can also be applied to other opto-electronic X-ray imaging systems.

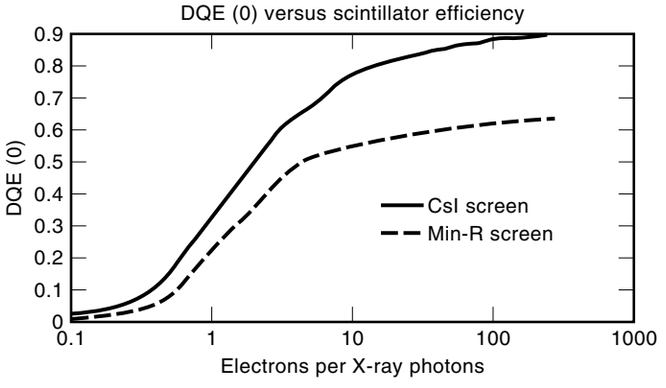

Figure 12. The effect of the quantum efficiency of the scintillating screen (h) on the X-ray quantum efficiency for the overall system. In this figure, DQE(0) curves of two optically coupled CCD systems using different scintillators are plotted as a function of the quantum efficiency of the scintillator screen (h) and total quantum gain (electronics per X-ray photon). Note that the DQE values presented in this figure represent the maximum achievable values.

BIBLIOGRAPHY

1. G. S. Shaber, C. Lockard, and J. Boone, High resolution digital radiography utilizing CCD planar array, *SPIE Proc.,* **914**: 262–269, 1988.
2. A. Karellas et al., Charge-coupled device detector: Performance considerations and potential for mammographic imaging, *Med. Phys.,* **19**: 1015–1023, 1992.
3. C. Kimme-Smith and T. Solberg, Acceptance testing prone stereotactic biopsy units, *Med. Phys.,* **21** (7): 1197–1201, 1994.
4. H. Liu et al., Optical properties of fiber tapers and their impact on the performance of a fiberoptically coupled CCD x-ray imaging system, *SPIE Proc.,* **1894**: 136–147, 1993.
5. H. Liu et al., Large-field high-spatial resolution digital x-ray mammography, *SPIE Proc.,* **2390**: 110–115, 1995.
6. M. F. Piccaro and E. Toker, Development and evaluation of a CCD-based digital imaging system for mammography, *SPIE Proc.,* **1901**: 109–119, 1993.
7. R. S. Nelson et al., An evaluation of a fluorescent screen-isocon camera system for x-ray imaging in radiology, *Med. Phys.,* **9**: 777–783, 1982.
8. A. Macovski, *Medical Imaging Systems,* Englewood Cliffs, NJ: Prentice-Hall, 1983.
9. H. Liu, Digital fluoroscopy with an optically coupled charge-coupled device, Ph.D. dissertation, Worcester Polytechnic Inst., Worcester, MA, 1992.
10. S. Shalve, Video techniques for portal imaging, *Comp. Med. Imag. Graph.,* **13** (3): 217–226, 1989.
11. G. T. Barnes and D. P. Chakraborty, Radiographic mottle and patient exposure in mammography, *Radiology,* **145**: 815–821, 1982.
12. A. Rose and P. K. Weimer, Physical limits to the performance of imaging systems, *Phys. Today,* **42** (9): 24–32, 1989.
13. S. M. Gruner, CCD and vidicon x-ray detectors: theory and practice, *Rev. Sci. Instrum.,* **60**: 1545–1551, 1989.
14. W. R. Brody, *Digital Radiography,* New York: Raven, 1984, p. 83.
15. C. E. Dick and J. W. Motz, Utilization of monoenergetic x-ray beams to examine the properties of radiographic intensifying screen, *IEEE Trans. Nucl. Sci.,* **NS-28**: 1554–1558, 1981.
16. H. Liu, A. Karellas, and L. Harris, Methods to calculate lens efficiency in optically coupled CCD x-ray imaging systems, *Med. Phys.,* **21**: 1193–1195, 1994.
17. A. D. A. Maidment and M. J. Yaffe, Analysis of the spatial-frequency-dependent DQE of the optically coupled digital mammography detectors, *Med. Phys.,* **21**: 721–729, 1994.
18. H. Roehrig et al., Signal, noise and detective quantum efficiency in CCD based x-ray imaging systems for use in mammography, *Proc. SPIE,* **2163**: 320–329, 1994.
19. R. M. Nishikawa and M. J. Yaffe, Signal-to-noise ratio properties of mammographic film-screen systems, *Med. Phys.,* **12**: 32–39, 1985.
20. R. M. Nishikawa and M. J. Yaffe, Model of the spatial-frequency-dependent detective quantum efficiency of phosphor screens, *Med. Phys.,* **17**: 894–904, 1990.

21. J. C. Dainty and R. Shaw, *Image Science,* Boston, MA: Academic Press, 1974, p. 312.
22. H. Liu et al., CCD-scanning techniques for full-size digital mammography, *Radiology,* **197**: 291, 1995.
23. D. L. Lee et al., Projection radiography with use of a direct conversion imaging array, *Radiology,* **197**: 358, 1995.
24. H. Liu et al., Contrast-detail detectability analysis: Comparison of a digital spot mammography system and an analog screen-film mammography system, Academic Radiology, **4**: 197–203, 1997.
25. A. Rose, The sensitivity performance of the human eye on an absolute scale, *J. Opt. Soc. Am.,* **38**: 196, 1948.
26. B. H. Hasegawer, The Rose model, in *The Physics of Medical X-Ray Imaging,* Madison, WI: Medical Physics, 1990.
27. R. Wagner and D. Brown, Unified SNR analysis of medical imaging systems, *Phys. Med. Biol.,* **30** (6): 489–518, 1985.
28. H. Liu et al., Lesion detectability considerations for an optically coupled CCD x-ray imaging system, *IEEE Trans. Nucl. Sci.,* **41** (4): 1506–1509, 1994.

Reading List

The following books are suggested for references on X-ray generation, X-ray tubes, and generators:

N. Dyson, *X-Rays in Atomic and Nuclear Physics,* 2nd ed., New York: Cambridge Univ. Press, 1990.

E. Krestel, *Imaging Systems for Medical Diagnostics,* Berlin: Siemens, 1990.

J. Seibert, G. Barnes, and R. Gould, *Specification, Acceptance Testing and Quality Control of Diagnostic X-Ray Imaging Equipment,* Woodbury, NY: Amer. Inst. Physics, 1994.

XIZENG WU
University of Alabama at Birmingham

HONG LIU
University of Virginia